Fuel 312 (2022) 122910

Contents lists available at ScienceDirect

Fuel

journal homepage: www.elsevier.com/locate/fuel

Full Length Article

Conditioning the volatile stream from biomass fast pyrolysis for the attenuation of steam reforming catalyst deactivation

Enara Fernandez [a], Laura Santamaria [a], Maite Artetxe [a], Maider Amutio [a], Aitor Arregi [a], Gartzen Lopez [a,b,*], Javier Bilbao [a], Martin Olazar [a]

[a] Department of Chemical Engineering, University of the Basque Country UPV/EHU, P.O. Box 644, E48080 Bilbao, Spain
[b] IKERBASQUE, Basque Foundation for Science, Bilbao, Spain

ARTICLE INFO

Keywords:
Biomass
Pyrolysis
Reforming
Spouted bed
Low cost catalysts

ABSTRACT

The fast deactivation of the reforming catalyst greatly conditions H_2 production from biomass. In order to alleviate this problem, use of conditioning catalysts in a previous conditioning step has been proposed to modify the pyrolysis volatile stream reaching the reforming catalyst. The experimental runs have been conducted in a two-step reactor system, which includes a conical spouted bed reactor for the continuous pinewood sawdust pyrolysis and an in-line fixed bed reactor made up of two sections: the conditioning and the reforming steps. Biomass fast pyrolysis was conducted at 500 °C and the reforming step at 600 °C. Different conditioning beds (inert sand, γ-Al_2O_3, spent fluid catalytic cracking (FCC) catalyst and olivine) were used for the conditioning of biomass pyrolysis volatiles and the influence their composition has on the performance and deactivation of a commercial Ni/Al_2O_3 reforming catalyst has been analyzed.

Considerable differences were noticed between the conditioning catalysts, with the reforming catalyst stability decreasing as follows depending on the type of material used: γ-Al_2O_3 > olivine > inert sand ≈ no guard bed > spent FCC catalyst.

The high acidity of γ-Al_2O_3 (with a high density of weak acid centers) is suitable for the selective cracking of phenolic compounds (mainly guaiacol and catechol), which are the main precursors of the coke deposited on the Ni active sites. Although H_2 production is initially lower, the reforming catalyst stability is enhanced. These results are of uttermost significance in order to step further in the scaling up of the in-line pyrolysis-reforming strategy for the direct production of H_2 from biomass.

1. Introduction

Biomass is a promising renewable source for the production of fuels, chemicals and H_2 [1–4] due to its availability and CO_2 neutral contribution. Besides, H_2 is a clean fuel whose potential as an energy carrier makes it a promising choice for its transformation into any form of energy for diverse end-use applications.

In recent decades, the progress of technological strategies for H_2 production from biomass has gained increasing attention in the literature [5–9]. Two types of routes are used for biomass conversion into H_2, as are thermochemical and biological processes [10]. Thus, biomass may be converted into H_2 through the following routes: i) water biophotolysis using micro-algae and cyanobacteria, ii) photofermentation, iii) dark-fermentation, and iv) hybrid reactor system [5]. The biological H_2 production (biohydrogen) from microorganism metabolism is a promising technology under development, in which renewable sources can be used for the sustainable production of H_2 [11,12]. Amongst the different routes for biomass valorization, thermochemical processes have merited especial consideration in the literature [8,13,14], particularly biomass steam gasification [15–19], fast pyrolysis [20,21], and the steam reforming of the bio-oil obtained in the pyrolysis process [22–25]. More recently, the alternative route of biomass pyrolysis and in-line catalytic steam reforming has attracted remarkable attention for the production of H_2 from biomass [26–31]. Most pyrolysis-reforming studies conducted in the literature have been performed in discontinuous mode using batch reactors. However, a great effort has been made in the recent years in order to implement a continuous feeding system, and therefore to step further in the scaling-up of this process.

The choice of a suitable catalyst for these processes is of uttermost significance for the viability of their industrial implementation.

* Corresponding author.
E-mail address: gartzen.lopez@ehu.eus (G. Lopez).

https://doi.org/10.1016/j.fuel.2021.122910
Received 20 July 2021; Received in revised form 18 November 2021; Accepted 8 December 2021
Available online 21 December 2021

Accordingly, primary catalysts, such as dolomite, olivine, γ-Al_2O_3 or spent fluid catalytic cracking (FCC) catalyst, have been widely investigated in biomass gasification [32–35]. Thus, several authors have reported the activity of dolomite and olivine for reforming and cracking reactions [36,37], whereas γ-Al_2O_3 is effective in tar decomposition and promoting H_2 production [38]. The utilization of a spent FCC catalyst is of special relevance, since it increases the lifetime of a refinery waste material [39,40].

Besides, commercial Ni-based catalysts have been extensively used in steam reforming processes, since these types of catalysts involve several advantages, such as their lower cost compared to noble based catalysts, as well as their high activity for breaking C − C and O − H bonds. However, their fast deactivation, mainly by coke deposition on the active sites, is a great challenge to face up. Accordingly, different strategies have been proposed with the aim of improving the activity and stability of the reforming catalyst, as are the use of different reactor configurations, the selection of suitable operating conditions or the optimization of the catalyst design based on supports and promoters [8,41–43].

The strategy proposed in this study to attenuate the fast catalyst deactivation lies in the modification of the feed into the reforming step, which may be conducted in the pyrolysis reactor itself or downstream by upgrading the bio-oil produced in the biomass pyrolysis. Thus, it is well established that certain bio-oil compounds reaching the reforming catalyst bed significantly influence the mechanisms of catalyst deactivation, particularly coke formation, and therefore the performance of the catalyst in the reforming step [44]. Although huge effort has been made to assess the catalyst performance and its deactivation causes in the steam reforming process, the highly complex bio-oil composition and the problems associated with its handling boosted use of bio-oil model compounds, such as ethanol, phenol, acetic acid, toluene, or their mixture [45–47]. Therefore, knowledge of the reforming catalyst performance and the main species responsible for catalyst deactivation by coke deposition under real process conditions is still limited.

Based on this background, this study pursues a dual objective. On the one hand, to enhance catalyst activity and stability in the reforming step in a tandem pyrolysis-reforming reactor by conditioning the biomass pyrolysis volatile stream using highly available and inexpensive catalysts. On the other hand, to provide a further understanding of the reactivity of the main bio-oil oxygenate compounds and their role in the deactivation of the reforming catalyst. The results obtained in this study will contribute to progressing towards the understanding of the main coke precursors in the reforming step and promoting the proposal of new strategies for improving catalyst stability, which are the main challenges to be faced in the industrial implementation of the pyrolysis-reforming process.

Accordingly, the production of H_2 from biomass (pinewood sawdust) has been carried out in a conical spouted bed reactor (CSBR) for the fast pyrolysis, and an in-line fixed bed reactor for the reforming of the volatiles produced [48]. For the conditioning of this stream, different low cost materials (inert sand, γ-Al_2O_3, a spent FCC (fluid catalytic cracking) catalyst and olivine) have been located prior to the reforming catalyst. Continuous biomass pyrolysis has been conducted in a conical spouted bed reactor (CSBR) and the volatiles formed have been transferred into a fixed bed reactor for their conditioning and reforming. Thus, the fixed bed reactor includes two reaction sections, the first one with the guard catalyst (conditioning step) and the second one with the steam reforming one. In a previous study, this reactor configuration revealed a high efficiency for the conversion of the volatiles derived from biomass pyrolysis into a hydrogen rich syngas, with catalyst deactivation being lower than when a fluidized bed reactor is used in the reforming step [48].

2. Experimental

2.1. Feedstock

The biomass used in this process was pinewood waste (pinus insignis), which was crushed and sieved to a particle size in the range from 1 to 2 mm. The ultimate and proximate analyses were determined in previous studies in a *LECO CHNS-932* elemental analyzer and in a *TGA Q5000IR* thermogravimetric analyzer, respectively [26,49]. An isoperibolic bomb calorimetry *(Parr 1356)* was used to determine the higher heating value. Table 1 summarizes the main biomass features. Fig. S1 in the Supplementary Information shows the TG profile of the pinewood sawdust.

2.2. Conditioning and characterization of guard and reforming catalysts

Four different low-cost materials have been used in this study as guard catalysts for the conditioning of the pyrolysis volatile stream, as are: i) inert silica sand *(Minerals Sibelco),* ii) olivine *(Minerals Sibelco)*, with basic character and active for reforming biomass-derived oxygenates, iii) spent FCC catalyst, supplied by *Petronor Refinery* in Muskiz, Spain, and iv) γ-Al_2O_3 *(Alfa Aesar)*. The spent FCC catalyst and the γ-Al_2O_3 are of acid character and active for cracking reactions [39].

Prior to use, the spent FCC catalyst was regenerated by calcination with air at 575 °C for 1 h in order to burn the coke deposited during its utilization in the refinery. The FCC catalyst particles were agglomerated by wet extrusion to obtain a particle size suitable for use in the fixed bed. Bentonite (50 wt%) was used as binder to confer mechanical and thermal resistance upon this catalyst. Subsequently, the extruded sample was dried overnight and calcined with air at 575 °C for 2 h. Then, the FCC catalyst was ground and sieved to a particle size in the 0.8–1.6 mm range. Similarly, olivine and γ-Al_2O_3 were also ground and sieved to attain the desired particle size (0.8–1.6 mm). The fraction of inert silica sand was also within this range.

These conditioning catalysts were characterized by N_2 adsorption–desorption, X-ray Fluorescence (XRF) spectrometry and NH_3-TPD. The characterization procedure has been described in the Supplementary Information.

The commercial catalyst used in the reforming reactor (ReforMax® 330 or G90-LDP), denoted as G90, was supplied by Süd Chemie. The selection of this catalyst is based mainly on its availability and reliability (without reproducibility problems in its preparation), since a significant amount of catalyst is needed in all the experimental runs. Moreover, commercial G90 and other similar commercial Ni/Al_2O_3 catalysts have been extensively used in the literature about the steam reforming of tar compounds [50,51], biomass and sewage sludge pyrolysis volatiles [52–56] and pyrolysis oils produced from waste plastics [57].

This commercial catalyst for CH_4 reforming was provided as perforated rings (19 × 16 mm), which were ground and sieved to a particle size in the 0.4–0.8 mm range. This particle size range showed a suitable

Table 1
Pinewood sawdust characterization.

Ultimate analysis (wt%)[a]	
Carbon	49.33
Hydrogen	6.06
Nitrogen	0.04
Oxygen[b]	44.57
Proximate analysis (wt%)[c]	
Volatile matter	73.4
Fixed carbon	16.7
Ash	0.5
Moisture	9.4
HHV (MJ kg^{-1})	19.8

[a] on a dry ash free basis
[b] by difference
[c] on an air-dried basis

performance in previous studies operating in fixed bed regime [48]. The chemical composition of G90 catalyst is based on NiO, whose nominal content is 14 wt%, apart from $CaAl_2O_4$ and Al_2O_3. The textural properties of the fresh catalyst determined by N_2 adsorption–desorption have been shown in previous studies [58,59]. Accordingly, the catalyst is a mesoporous material, with mean pore diameter of 12.2 nm. The results of BET surface area (19.0 $m^2\ g^{-1}$) are rather low.

The Ni based catalyst reduction temperature was ascertained by temperature programmed reduction (TPR), and the results are provided elsewhere [60,61]. Accordingly, the TPR profile revealed two main peaks with the prevailing one located at 550 °C, which was ascribed to the reduction of NiO which is interacting with Al_2O_3 support. The peak observed at higher temperature (700 °C) was associated with $NiAl_2O_4$ spinel phase. Moreover, prior to the pyrolysis-reforming experiments, in-situ catalyst reduction was carried out by feeding a stream of 10 vol% H_2 with N_2 at 710 °C for 4 h.

2.3. Experimental equipment

The biomass pyrolysis-reforming has been carried out in a bench scale laboratory plant, whose scheme is shown in Fig. 1. The pyrolysis step was conducted in a conical spouted bed reactor (CSBR), whereas a fixed bed reactor was selected to perform the catalytic reforming of the volatiles from the pyrolysis step. In the latter reactor, different conditioning beds (sand, γ-Al_2O_3, FCC and olivine) were placed prior to the reforming catalyst bed (see Fig. 1).

Previous studies conducted by the research group have proven the good performance of the CSBR for the pyrolysis of different materials, such as biomass [49,62,63], waste plastics [64,65] or tires [66–68]. Moreover, the design of the CSBR is based on previous hydrodynamic studies [69], and its dimensions are as follows: conical section height, 73 mm; cylindrical section diameter, 60.3 mm; conical section angle, 30°; bed bottom diameter, 12.5 mm; and gas inlet diameter, 7.6 mm. Continuous removal of the char particles in this reactor is carried out by means of a lateral outlet pipe located above the bed surface (Fig. 1). The gas stream is heated to the desired temperature prior to entering the reactor by means of a preheater. Both the reactor and the gas preheater are located inside a radiant oven of 1250 W.

The temperature in the fixed bed reactor, which is located inside an oven (550 W), is controlled by a thermocouple located in the catalyst bed. The pilot plant is provided with a cyclone, which retains the char and sand particles entrained from the pyrolysis bed. With the aim of avoiding steam and heavy compounds condensation, both reactors (the CSBR and the fixed bed reactor), all interconnection pipes and the cyclone are placed inside a forced convection oven, wherein the box temperature is maintained at 300 °C. Avoiding the condensation of heavy compounds before and after the fixed bed reactor is essential to carry out the analysis of the products.

The solid feeding device consists of a vessel equipped with a vertical shaft connected to a piston placed below the material bed. At the same time as the piston raises, the biomass feeder is vibrated, which ensures continuous discharge of the biomass into the reactor.

The water required in the conical spouted bed and in the reforming step was fed by a high precision pump (Gilson 307). It was vaporized by means of an electric heater prior to entering the pyrolysis reactor. Moreover, the plant is provided with three mass flow-meters for N_2, (used as fluidizing agent in the process of heating the reaction system), air and H_2 (used for the reforming catalyst reduction prior to the reforming step).

The product condensation system is provided with a condenser and a coalescence filter, which ensure the collection of the non-reacted steam and bio-oil compounds prior to analysis.

2.4. Experimental conditions and product analysis

The pyrolysis step was carried out at 500 °C, as the condensable volatile fraction (liquid fraction) obtained in the biomass pyrolysis is maximized at this temperature [49]. Based on previous hydrodynamic

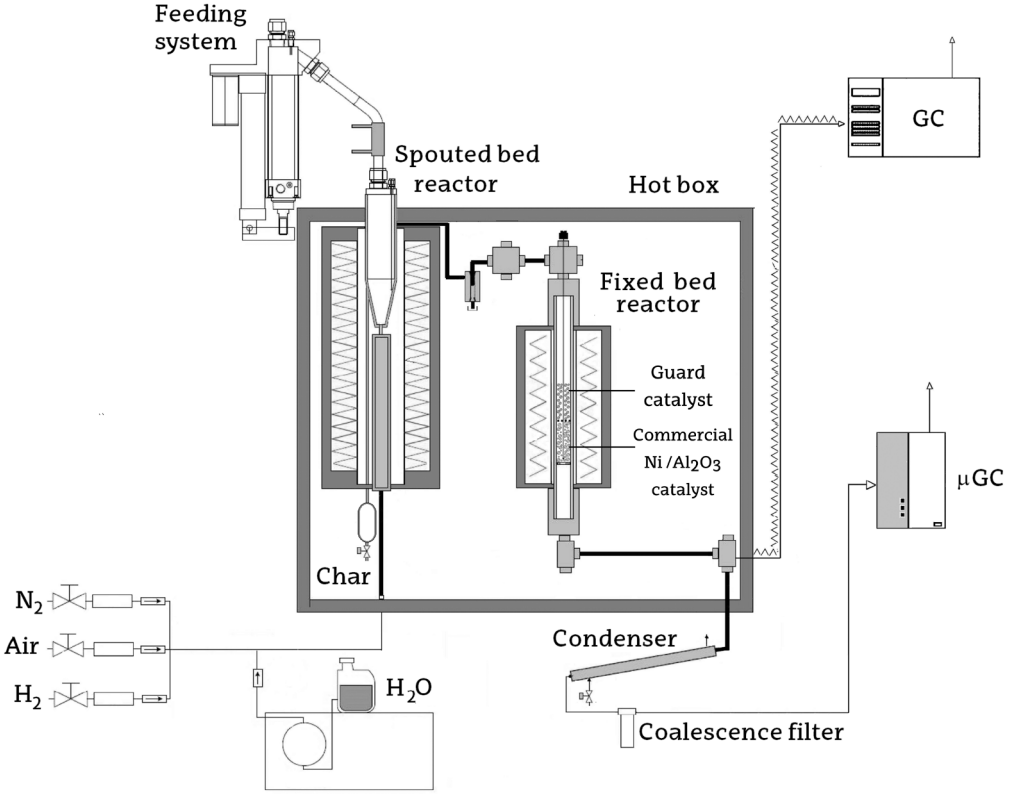

Fig. 1. Scheme of the pyrolysis-reforming laboratory scale plant.

studies, the CSBR contained 50 g of silica sand with a particle size in the 0.3–0.35 mm range. Besides, a water flow rate of 3 mL min^{-1} was chosen for all the runs, which corresponds to a steam flow rate of 3.73 NL min^{-1}. These conditions ensure a vigorous movement in the CSBR.

The reforming temperature was fixed at 600 °C, which was established as the optimum one in previous biomass pyrolysis-reforming runs [26]. Thus, higher temperatures (700 °C) showed a limited effect on the reforming results [58] and may favour sintering of the metallic Ni active sites. [70].

In the fixed bed reactor, the bed was divided into two sections: i) the conditioning step with the guard bed, (silica sand, γ-Al_2O_3, spent FCC catalyst or olivine), which is located in the upper section of the reactor, and ii) the reforming catalyst bed, which is composed of a mixture of inert sand (1–2 mm) and a commercial Ni/Al_2O_3 (G90) catalyst (0.4–0.8 mm). A steel mesh was used to divide both fractions with the aim of easing their separation for further characterization when each experimental run was finished.

The conditioning catalysts used in this study are significantly different concerning density, i.e., sand: 2600 kg m^{-3}; olivine: 3300 kg m^{-3}; FCC: 1246 kg m^{-3}, and γ-Al_2O_3: 1666 kg m^{-3}. The bed mass of these materials was chosen in order to have the same bed volume in all the experiments (30 mL), which was that corresponding to a $GHSV_{volatiles}$ of 3100 h^{-1}, and the particle size of all guard catalysts was in the 0.8–1.6 mm range. The corresponding masses were 44.2 g of silica sand, 46.2 g of olivine, 17.3 g of spent FCC catalyst and 19.9 g of γ-Al_2O_3. Moreover, the same bed volume of the mixture of commercial Ni/Al_2O_3 catalyst (G90) and inert sand was used (30 mL), which corresponds to 9.4 g and 29.0 g of reforming catalyst and inert sand, respectively.

In order to compare the influence of the conditioning step on the reforming one, the same operating conditions were established. Accordingly, all the runs were conducted in continuous regime by feeding 0.75 g min^{-1} of biomass, with the S/B ratio being 4 and the space time 15 g_{cat} min $g_{volatiles}{}^{-1}$. These conditions allow attaining conversion values close to thermodynamic equilibrium without involving high energy requirements to vaporize the water supplied. Thus, given that the steam flow rate required for attaining a suitable spouting regime in the CSBR has been set at 3.73 NL min^{-1} (3 mL min^{-1} of water), the corresponding biomass flow rate was 0.75 g min^{-1}.

Prior to the pyrolysis-reforming runs, all the elements of the plant were heated using N_2 as fluidizing agent. Then, the fluidizing gas was switched to water and once temperature had been stabilized, biomass feed started.

The analysis of the volatile stream was carried out at three different locations: i) after the pyrolysis step, ii) once the stream had passed the guard bed (conditioning step) and, finally, iii) at the outlet of the steam reforming reactor. Furthermore, experimental runs using different reactor configurations have been conducted under the same conditions. Thus, in the pyrolysis runs, the volatile stream is directly connected to the condensation system without passing through the fixed bed. In the conditioning runs, both reactors (pyrolyser and conditioning fixed bed) were used, with the fixed bed containing the conditioning catalyst, i.e., the reforming catalyst G90 was not introduced in the reactor. Finally, the configuration for the pyrolysis-reforming runs was made up of a CSBR and a fixed bed reactor containing both the guard and the reforming catalysts. This latter configuration corresponds to the scheme shown in Fig. 1.

The mass balance in the pyrolysis runs (biomass pyrolysis and biomass pyrolysis + guard catalyst) was closed by weighting the char particles, i.e., the amount of char remained in the reactor plus those collected through the lateral pipe and retained in the cyclone and filter, and combining this information with that obtained by on-line chromatographic analysis. In these pyrolysis runs, cyclohexane was used as an internal standard to validate the mass balance closure. Thus, the pyrolysis product stream leaving the fixed bed reactor was analyzed in-line in a GC Agilent 6890 provided with a HP-Pona column and a flame ionization detector (FID) by means of a line thermostated at 280 °C, and the non-condensable gases were analyzed in a GC Varian 4900. Besides, the identification of the bio-oil compounds was conducted by condensation of the liquid sample and further analysis by means of a GC–MS spectrometer (Shimadzu 2010-QP2010S) provided with a BPX-5 column. In the pyrolysis-reforming runs, the overall and elemental mass balances (C, H and O) were closed based on the information about the volatile stream that reached the reforming catalyst (which has been determined as mentioned above) and the information obtained in the GC and microGC analyses of the stream at the outlet of the reforming step. The mass balances closure was above 95 % in all cases, and runs were repeated at least 3 times in order to ensure reproducibility. The chromatographic analyses were conducted in-line by means of a GC Agilent 6890 provided with a HP-Pona column and a flame ionization detector (FID). In order to avoid the condensation of non-converted oxygenate compounds, the sample from the reforming reactor outlet stream has been injected into the GC by means of a line thermostated at 280 °C. The permanent gases, i.e., H_2, CO_2, CO, CH_4 and C_2-C_4 hydrocarbons, were analyzed in a GC Varian 4900 once the outlet stream of the reforming reactor was condensed and filtered.

2.5. Characterization of the deactivated conditioning and reforming catalysts

The textural properties of all conditioning beds were analyzed after each experimental run by N_2 adsorption–desorption technique in a *Micromeritics ASAP 2010* following the procedure described in the Supplementary Information.

The coke formed on the spent catalysts, both guard and reforming ones, was analyzed at the end of each continuous run. The coke content was measured by Temperature Programmed Oxidation (TPO) in a Thermobalance (T*GA Q5000 TA Instruments*) coupled to a mass spectrometer (*Thermostar Balzers Instrument*). Given that the Ni active phase is oxidized at the same time as the coke combustion occurs, the CO_2 formation is monitored throughout the TPO runs, according to the following procedure: i) Signal stabilization with a N_2 stream at 100 °C, and, ii) oxidation with air (heating rate of 5 °C min^{-1} to 800 °C maintaining this temperature for 30 min to ensure complete coke combustion. Similarly, the amount of coke deposited on each guard catalyst after the pyrolysis-reforming runs was determined following the same procedure. The deactivated G90 catalysts were analyzed by Scanning Electron Microscopy (SEM) in a JEOL JSM-6400 apparatus.

2.6. Reaction indices

In order to evaluate the influence the different guard catalysts have on the subsequent reforming step, volatile conversion and individual product yields have been taken as the key reaction indices. It should be noted that the definition of these reaction indices is based on the volatile products that reach the commercial Ni/Al_2O_3 catalyst (G90) bed (gases and bio-oil derived compounds), i.e., once the volatile stream from the pyrolysis step had passed the guard bed. Thus, the carbon contained in the char produced in the pyrolysis step was not considered, given that this product was removed from the CSBR (through the lateral pipe) prior to the conditioning step.

Accordingly, the volatile conversion in the reforming step is determined as the ratio between the C moles in the product stream leaving the reforming step (C_{gas}) and the C moles in the volatile stream reaching the reforming catalyst ($C_{volatiles}$):

$$X = \frac{C_{gas}}{C_{volatiles}} \cdot 100 \quad (1)$$

Similarly, the yield of each individual product, i, has been calculated based on the pyrolysis volatile stream.

$$Y_i = \frac{F_i}{F_{volatiles}} \cdot 100 \quad (2)$$

where Fi and Fvolatiles are the molar flow rates of each compound i and the volatile stream at the inlet of the reforming reactor, respectively.

The hydrogen yield is defined based on the maximum allowable by stoichiometry:

$$Y_{H_2} = \frac{F_{H_2}}{F^0_{H_2}} \cdot 100 \quad (3)$$

where F_{H2} is the H_2 molar flow rate and F^0_{H2} the maximum allowable by the following stoichiometry:

$$C_nH_mO_k + (2n-k)H_2O \rightarrow nCO_2 + (2n+m/2-k)H_2 \quad (4)$$

Finally, H_2 production is defined by mass unit of the biomass in the feed:

$$P_{H_2} = \frac{m_{H_2}}{m^0_{biomass}} \cdot 100 \quad (5)$$

where m_{H2} and $m^0_{biomass}$ are the mass flow rates of the H_2 produced and biomass fed into the process, respectively.

3. Results

3.1. Conditioning catalyst characterization

The textural properties (BET surface area, pore volume and pore diameter) of the conditioning catalysts are shown in Table 2. As observed, FCC and γ-Al_2O_3 are mesoporous materials, with an average pore size of around 17.0 nm, whereas inert sand and olivine are non-porous materials with negligible BET surface area and pore volume. Apart from the characteristic features of the conditioning catalysts, their physical properties may significantly influence the pyrolysis volatile composition to be fed into the reforming catalyst bed. Thus, mesoporosity would enhance the diffusion of bulky reactants, i.e., phenolic compounds, such as guaiacol and their derivatives [71]. In the case of the spent FCC catalyst, which is based on the HY zeolite, the use of bentonite as binder provides meso and macropores to the catalyst, which minimize external blockage of the channels [72]. However, the microporous structure of this zeolite is also evident, with a microporous surface area of 57 $m^2\ g^{-1}$.

Table 2
Properties of the conditioning catalysts.

	Sand	γ-Al_2O_3	FCC	Olivine
Physical properties				
S_{BET} ($m^2\ g^{-1}$)	0.6	100.6	81.3	2.4
$S_{micropore}$ ($m^2\ g^{-1}$)	1.1	11.5	56.7	0.7
V_{pore} ($cm^3\ g^{-1}$)	–	0.42	0.09	0.003
d_{pore} (nm) BJH	–	16.9	16.8	–
Chemical properties				
NiO (wt%)	–	–	0.05	–
MgO (wt%)	–	–	1.09	48.79
SiO_2 (wt%)	98.0	0.02	53.93	43.18
Fe_2O_3 (wt%)	–	–	2.10[a]	7.68
CaO (wt%)	–	–	0.24	0.12
Al_2O_3 (wt%)	–	99.98	31.90	0.04
Na_2O (wt%)	–	–	0.38	0.06
TiO_2 (wt%)	–	–	0.85	0.02
MnO (wt%)	–	–	0.01	0.11
P_2O_5 (wt%)	–	–	0.22	–
V_2O_5 (wt%)	–	–	0.20	–
K_2O (wt%)	–	–	0.24	–
La_2O_3 (wt%)	–	–	1.25[b]	–
SO_3 (wt%)	–	–	0.13	–
Cl (wt%)	–	–	0.15[b]	–
Acidity				
Total acidity ($\mu mol_{NH3}\ g_{cat}^{-1}$)	–	106.32	46.73	6.17

[a] Expressed as total Fe_2O_3.
[b] Determined by semi-quantitative software.

The chemical composition of each conditioning catalyst was determined by XRF analysis, and the results are set out in Table 2. As observed, inert sand is mainly composed of SiO_2; olivine is a mineral containing MgO, SiO_2 and Fe_2O_3; the γ-Al_2O_3 used in this study contains a small amount of SiO_2, apart from Al_2O_3; and the FCC catalyst agglomerated with bentonite (50 wt%) is a mixture containing Al_2O_3, SiO_2, Fe_2O_3 and P_2O_5, among other metal oxides. Futhermore, incorporation of bentonite greatly influences the composition of the spent FCC catalyst (used in a previous gasification study [39]), as it leads to a significant increase in the amount of SiO_2. Moreover, it has been widely reported that the chemical composition of the olivine plays a positive role in tar decomposition and reforming reactions [73,74] due to the presence of Fe^0 on its surface [75].

Table 2 also shows the total acidity of the conditioning catalysts determined by NH_3-TPD analysis. The results obtained revealed that only the spent FCC and the γ-Al_2O_3 catalyst contain acid sites, with a total acidity of 47 and 106 $\mu mol_{NH3}\ g_{cat}^{-1}$, respectively, whereas in the case of olivine, a negligible acidity is observed (6 $\mu mol_{NH3}\ g_{cat}^{-1}$). The acidity of these materials enhances cracking reactions involving bio-oil oxygenated compounds, leading to a higher amount of aromatics and paraffins.

3.2. Biomass pyrolysis and catalytic conditioning

Biomass pyrolysis was conducted at 500 °C using steam as fluidizing agent. Moreover, the catalytic conditioning of fast pyrolysis volatiles was carried out at 600 °C in the fixed bed reactor (see Fig. 1). A previous study detailed the biomass pyrolysis products obtained using these low-cost conditioning catalysts, and the main mechanisms of bio-oil transformation [76].

The pyrolysis products obtained were grouped into three different fractions: i) a gaseous fraction made up of CO_2, CO, H_2 and small amounts of C_1–C_4 hydrocarbons, ii) a condensable volatile fraction (liquid fraction or bio-oil) composed of water and a complex mixture of oxygenated compounds, and iii) a solid residue or char, which is the non-volatilized biomass fraction. Table 3 shows the product yields obtained once the pyrolysis stream obtained at 500 °C in the CSBR had passed the conditioning beds in the fixed bed reactor at 600 °C.

As observed in Table 3, a high bio-oil yield was obtained in the biomass pyrolysis at 500 °C (75.36 wt%), which evidences the good performance of the CSBR for biomass pyrolysis due to the characteristic features of this reactor, as are high heating rates, short vapour residence times and rapid char removal from the hot reaction environment [49,77,78]. Conditioning catalysts led to a significant reduction in the bio-oil yield at the expense of gaseous product formation. In the case of inert sand, this drop is a consequence of thermal cracking reactions, whereas the decrease with the other catalytic materials is due to simultaneous thermal and catalytic cracking reactions. These results evidence that the features of the conditioning catalysts, i.e., physical

Table 3
Effect of conditioning catalysts on the product yields (wt%).

	Pyrolysis 500 °C	Inert sand	γ-Al_2O_3	FCC	Olivine
Gas	**7.30 ± 0.29**	**14.37 ± 0.62**	**32.45 ± 1.27**	**26.11 ± 0.96**	**18.89 ± 0.66**
CO	2.25	6.51	16.71	11.96	7.10
CO_2	4.68	6.37	10.72	11.25	9.67
CH_4	0.19	0.99	2.01	1.34	0.86
C_2-C_4	0.12	0.37	2.66	1.41	0.87
H_2	0.06	0.12	0.34	0.14	0.40
Bio-oil	**75.36 ± 2.83**	**68.29 ± 2.39**	**50.21 ± 1.61**	**56.55 ± 2.32**	**63.77 ± 2.49**
Char	**17.34 ± 0.81**	**17.34 ± 0.81**	**17.34 ± 0.81**	**17.34 ± 0.81**	**17.34 ± 0.81**

properties, chemical composition and catalyst acidity (see Table 2), greatly influence the composition of the volatile stream to be fed into the reforming catalyst bed. Thus, although all conditioning catalysts tested are active for cracking (with an increase in the non-condensable gas yield in detriment of the condensable fraction (bio-oil)), the basic nature of olivine, as well as its limited porous structure (which hinders the diffusion of bulky oxygenated compounds into the bed material), led to a lower extension of cracking reactions. Besides, the mesoporous structure of FCC and Al_2O_3 guard catalyst, and especially the higher acidity of FCC and γ-Al_2O_3 catalysts, Table 2, led to higher gas yields (26.11 and 32.45 wt%, respectively) due to the promotion of bio-oil cracking.

The char produced is continuously extracted from the pyrolysis reactor by a lateral outlet (see Fig. 1), and its yield was not therefore affected by conditioning catalysts. Accordingly, it remained constant in all the experimental runs (17.34 wt%).

In the biomass pyrolysis at 500 °C, CO and CO_2, and small amounts of H_2 and C_1–C_4 hydrocarbons account mainly for the gaseous product stream. Besides, when inert sand, spent FCC and γ-Al_2O_3 were used, CO was the main compound in the non-condensable gaseous stream, which is evidence that decarbonylation reactions prevailed rather than decarboxylation ones. The higher extent of cracking reactions when spent FCC and γ-Al_2O_3 catalysts were used was also evidenced in the higher yield of CH_4 and C_2-C_4 hydrocarbons in the volatile stream. However, in the case of olivine, the yield of CO_2 was higher than that of CO and the other gaseous compounds due to the basic nature of this mineral, which enhanced ketonization and aldol condensation reactions leading to the formation of CO_2 and water [79]. Besides, the highest H_2 yield was observed in the experimental runs conducted with the olivine guard bed. Thus, the chemical composition of olivine, which contains Fe^0 on its surface, promotes reforming and WGS reactions [73,75].

The detailed bio-oil composition obtained in each experimental run is shown in Table 4. The inert nature of steam as fluidizing agent in the biomass pyrolysis at 500 °C has been demonstrated in previous studies [26,80], and has been confirmed in this one by comparing the results obtained when steam was used as fluidizing agent (see Tables 3 and 4) with those reported for N_2 [49]. Besides, this inert nature of steam is a great advantage for process viability, as the cost of the gases is reduced and the problems related to inert gas separation prior to the catalytic reforming step are avoided. However, the use of conditioning beds significantly modified the composition of the bio-oil products. As aforementioned, all conditioning catalysts were located in a fixed bed reactor at 600 °C (above that of pyrolysis), which may also have certain influence on the bio-oil composition.

Table 4
Effect of conditioning catalysts on the bio-oil composition (wt.%).

	Pyrolysis 500 °C	Inert sand	γ-Al_2O_3	FCC	Olivine
Acids	4.00	4.06	0.00	0.00	2.26
Aldehydes	3.29	5.41	1.10	0.52	3.78
Ketones	9.64	9.23	4.23	4.76	9.65
Alcohols	2.43	0.69	0.00	0.00	0.49
Polycyclic Aromatic Alcohols	0.27	2.47	6.52	8.45	6.66
Phenols	21.98	17.45	15.94	17.92	13.14
Alkyl-phenols	2.16	2.33	15.94	5.24	2.73
Catechols	10.99	5.60	0.00	11.56	6.62
Guaiacols	8.84	9.52	0.00	1.12	3.76
Furans	3.10	3.32	0.62	3.05	1.41
Saccharides	6.03	4.11	0.00	0.00	4.22
Hydrocarbons	0.00	0.06	8.49	6.12	1.06
Non-aromatics	0.00	0.06	0.69	0.00	0.03
Light aromatics (BTX)	0.00	0.00	0.69	0.31	0.03
PAHs	0.00	0.00	7.12	5.80	0.99
Others	0.09	0.00	0.00	0.15	3.15
Unidentified	16.74	15.68	13.03	13.37	15.60
Water	32.44	37.52	50.08	45.67	38.59

In comparison with the bio-oil obtained in the pyrolysis at 500 °C, the use of inert sand led to a significant drop in the amount of light alcohols, saccharides, and mainly in that of the phenolic fraction (particularly the catechol fraction), as a result of thermal cracking reactions. Moreover, the concentration of polycyclic aromatic alcohols increased from 0.27 to 2.47 wt%, respectively. The acidity of the spent FCC and γ-Al_2O_3 conditioning catalysts (Table 2) promoted deoxygenation reactions, as well as cracking, oligomerization, alkylation, isomerization, cyclization and aromatization, leading to a considerable increase in the hydrocarbon fraction (to 6.12 and 8.49 wt%, respectively). Significant differences were observed in the distribution of the components in the phenolic fraction, with catechols being the major components with the FCC conditioning bed, whereas the phenolic fraction obtained with the Al_2O_3 catalyst only contained alkyl-phenols. The higher selectivity of the Al_2O_3 catalyst for the production of alkyl-phenols revealed the effective dealkoxylation of guaiacols and cathecols [81].

In the case of the olivine conditioning bed, a decrease in the acid and furan fractions was observed, with the ketone fraction remaining almost constant. Thus, the basic nature of this material promoted the ketonization of acids over basic catalysts, as well as the aldol condensation of small ketone and aldehyde molecules to larger chain ketones by carbon–carbon coupling reactions [79,82]. A reduction in the guaiacol fraction, and therefore in the overall phenolic fraction was also evidenced, whereas the yield of hydrocarbons (mainly naphthalene compounds) increased because of secondary cracking reactions.

3.3. Effect of the conditioning beds on the activity and stability of the reforming catalyst

The effect of using conditioning catalysts prior to the reforming step has been analyzed, i.e., the influence the composition of the volatile stream fed into the reforming bed has on the catalyst activity and stability. Accordingly, the evolution of the volatile conversion (Fig. 2) and product yields (Fig. 3) was monitored with time on stream based on the following main reactions:

Oxygenate steam reforming:

$$C_nH_mO_k+(n-k)H_2O \rightarrow nCO + (n + m/2-k)H_2 \quad (6)$$

Water Gas Shift (WGS):

$$CO + H_2O \leftrightarrow CO_2 + H_2 \quad (7)$$

Oxygenate cracking (secondary reaction):

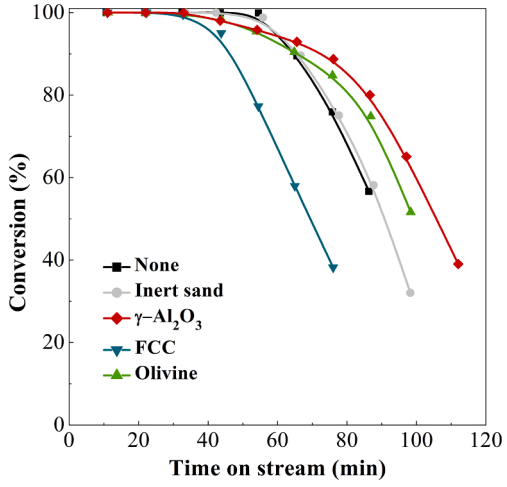

Fig. 2. Effect of the conditioning bed addition on the evolution of oxygenate conversion with time on stream in the reforming of biomass pyrolysis products.

$C_nH_mO_k \rightarrow$ oxygenates + hydrocarbons + CH_4 + CO + CO_2 + C (8)

Methane (and hydrocarbons) steam reforming:

$CH_4 + H_2O \leftrightarrow CO + 3H_2$ (9)

Fig. 2 shows that the volatiles derived from biomass pyrolysis are completely reformed independently of the stream composition at the inlet of the reforming catalyst bed, which is explained by the high activity of the commercial Ni/Al_2O_3 (G90) catalyst.

It is to note that the volatile stream reaching the reforming catalyst in any experimental run is made up of a complex mixture of oxygenate compounds. Most of the research studies dealing with the mechanisms involving reforming reactions and/or catalyst deactivation have been

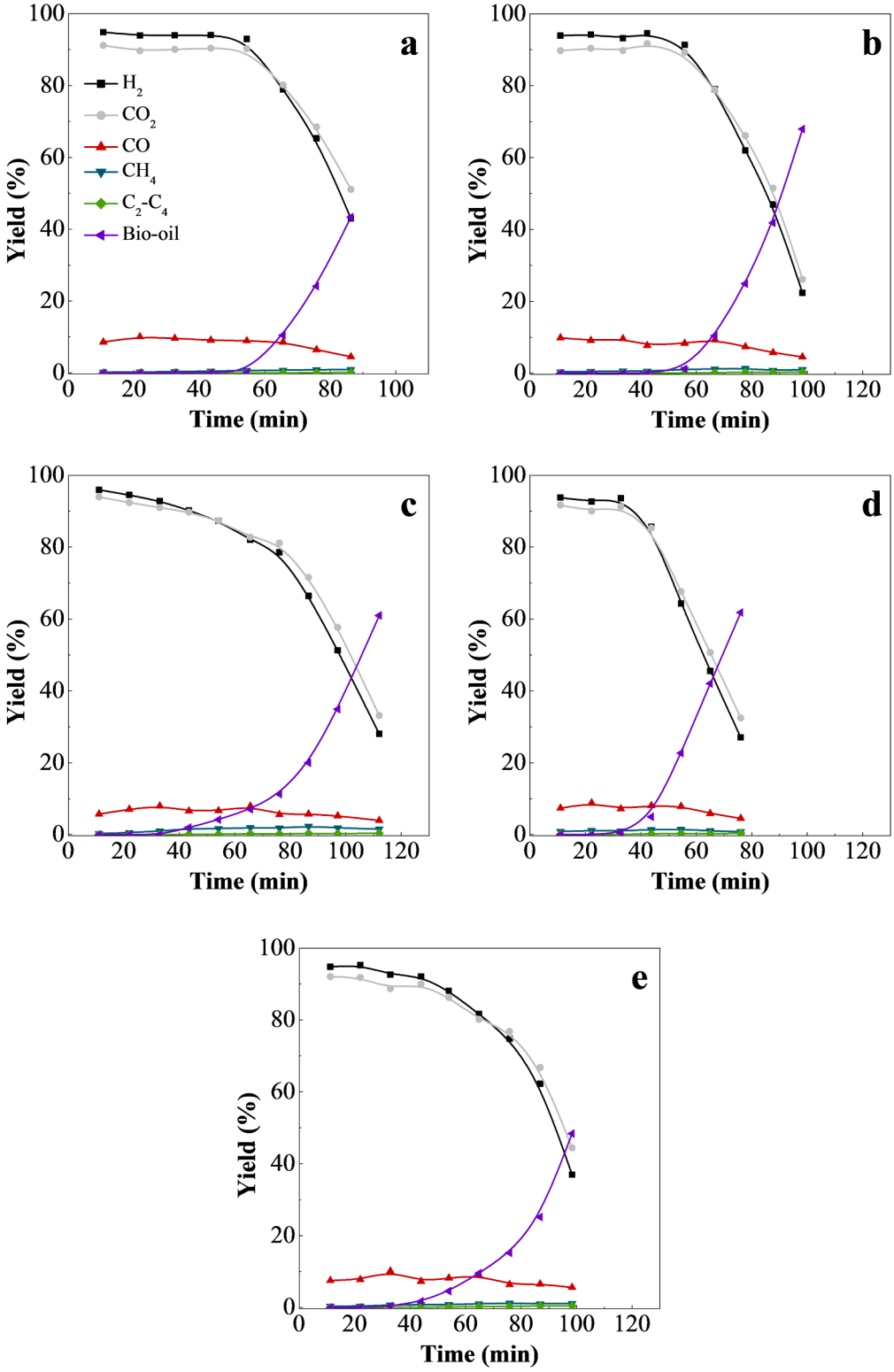

Fig. 3. Effect of the conditioning bed addition on the evolution of the individual product yields with time on stream in the reforming step. a) Without conditioning bed; b) Inert sand; c) γ-Al_2O_3; d) FCC and, e) Olivine.

conducted with model compounds and synthetic mixtures simulating bio-oil and tar. However, different compounds reactivity has been reported depending on whether they are reformed alone or in a mixture of different oxygenated compounds [83]. Therefore, detailed and laborious studies are required to analyse, on the one hand, the reactivity of the compounds in the biomass pyrolysis volatile stream modified by the use of conditioning catalysts (due to the high amount of species contained and their interactions) and, on the other hand, their further contribution to catalyst deactivation.

As observed in Fig. 2, the experiments conducted without any conditioning catalyst showed a stable catalyst performance for the first 50 min on stream (conversion values up to 99.8 %), and it then decreased to 56.6 % after 86 min on stream, which is evidence of the deactivation of the catalyst. The runs conducted with inert sand as guard bed showed similar results of conversion, which decreased to 58.2 % for 87 min on stream. Despite the differences obtained in the volatile composition when no conditioning catalyst and inert sand were used (see Table 4), similar catalytic performance in the reforming step was observed. It seems that, in the pyrolysis-reforming experiment without any conditioning material, the volatile stream leaving the pyrolysis reactor undergoes thermal cracking reactions in parallel with catalytic ones on the reforming catalyst, with the thermal cracking leading to a volatile composition similar as the one obtained with inert sand.

Regarding the experiments conducted using olivine guard bed, almost full conversion was attained for the first 30 min on stream, and it then gradually decreased to 51.6 % for 98 min on stream. However, despite the fact that the reforming catalyst begins to lose activity earlier when there is an olivine guard bed than without any conditioning catalyst or inert sand, its deactivation rate is significantly lower, which leads to greater stability over time. This fact is explained by the different nature of the volatile stream to be reformed. The presence of more refractory compounds in the volatile stream when olivine was used as conditioning catalyst, namely the hydrocarbon fraction (1.06 wt%), led to a faster initial loss of activity. Although the hydrocarbon fraction's reactivity is low for reforming reactions, its low concentration did not involve a fast catalyst deactivation with time on stream. Other authors have also reported a higher reactivity of oxygenated compounds derived from biomass pyrolysis in comparison with the hydrocarbon compounds due to the presence of C=O bonds that enhance the formation of carbon oxides in the reforming step [84,85]. The lower amount of phenolic compounds when olivine was used, especially the guaiacol fraction, resulted in a greater stability over time. The lower aldehyde fraction than with inert sand may also contribute to attenuating catalyst deactivation. Thus, several authors have reported that the main coke precursors, and therefore the main responsible for catalyst deactivation are aldehydes, phenols, and saccharides [83,86]. Gayubo et al. [86] state phenolic compounds (as well as aldehydes) are the main contributors to catalyst deactivation by coke formation. Valle et al. [87] analyzed the influence the presence of phenolic compounds has on catalyst stability in the reforming of raw bio-oil. Accordingly, they approached the removal of these phenolic compounds from the raw bio-oil by accelerated aging and liquid–liquid extraction methods. They observed that catalyst deactivation was lower than when raw bio-oil was used in the steam reforming, since phenols removal from the bio-oil significantly reduced coke content. Ochoa et al. [88] associated the composition of oxygenate compounds in the reaction medium with the composition of the coke formed using Fourier transform infrared (FTIR) spectroscopy. They concluded that methoxyphenols (guaicols) and levoglucosan (saccharides) have greater influence on coke formation than acids, ketones and aldehydes.

The performance of the commercial Ni/Al_2O_3 (G90) catalyst when the spent FCC guard catalyst was used showed full conversion for the first 30 min on stream, and then sharply decreased attaining a conversion value of 38.2 % after 76 min on stream. This fast catalyst deactivation is mainly associated with the high concentration of the phenolic fraction, especially the high amount of catechol compounds (11.56 wt %). Besides, the high concentration of polycyclic aromatic alcohols (mainly composed of indenol and naphthalenol derived compounds) may also contribute to the fast catalyst deactivation in the reforming step. These results are consistent with those obtained in other literature studies. Thus, Artetxe et al. [47] investigated the steam reforming of different tar model compounds (phenol, toluene, methyl naphthalene, indene, anisole and furfural), and reported that the lowest conversion was attained when phenol was used as model compound. Trane-Restrup and Jensen [89] studied the steam reforming of cyclic model compounds in the bio-oil (2-methylfuran, furfural, and guaiacol) over Ni-based catalysts, revealing that the phenolic compound guaiacol was the most difficult to convert to synthesis gas. Likewise, Wang et al. [90] reported the lower reactivity of phenol over a Ni based catalyst compared to other oxygenated compounds, such as furfural, hydroxyacetone or acetic acid.

The high concentration of hydrocarbons (6.12 wt%) in the bio-oil as a result of the acidity of the FCC catalyst also influenced the reforming reaction. This hydrocarbon fraction is mainly composed of polycyclic aromatic hydrocarbons (PAHs), namely, indene (0.12 wt%), naphthalene (2.40 wt%), fluorene (0.74 wt%), anthracene (0.65 wt%) and phenanthrene (1.89 wt%). Thus, several authors have reported the lower reactivity of large cyclic hydrocarbons with higher molecular weights than oxygenate compounds in the steam reforming reactions [47,84]. Regarding hydrocarbon reactivity in steam reforming reactions, several studies in the literature report lower reactivity of naphthalene than other bio-oil model compounds like toluene, benzene, pyrene or anthracene [41,91,92]. In fact, these aromatic hydrocarbons are well known because they undergo condensation reactions to form coke, which accelerates catalyst deactivation [93,94].

The best catalytic performance was observed when γ-Al_2O_3 was used as conditioning catalyst, with a stable volatile conversion for the first 30 min on stream and then decreasing to 39 % subsequent to 112 min on stream. Similarly to other conditioning catalysts, the initial loss of catalyst activity occurred earlier than in the runs conducted without conditioning bed or with silica sand, which is a consequence of the total acidity of the γ-Al_2O_3, as it promotes secondary cracking reactions leading to a higher concentration of olefins and aromatic hydrocarbon compounds. However, although there is a high concentration of this hydrocarbon fraction (the highest one is obtained when Al_2O_3 is used as conditioning bed), these compounds do not involve a sharp decrease in volatile conversion. The reduction in the concentration of phenols in the volatile stream to be reformed, particularly that of guiacol and catechol fractions, significantly attenuated the Ni/Al_2O_3 (G90) catalyst deactivation. Total removal of acids and saccharides and a significant reduction in the aldehyde fraction may also contribute to attenuating the fast deactivation of the reforming catalyst. Several authors have reported that the main coke precursors, and therefore the main responsible for catalyst deactivation, are aldehydes, phenols, and saccharides [83,86].

The great differences in the performance of the reforming catalysts when the spent FCC catalyst and γ-Al_2O_3 conditioning catalysts were used are mainly due to the differences observed in the composition of phenolic compounds. Thus, whereas alkyl-phenols (15.96 wt%) are only obtained with the γ-Al_2O_3, catechols are the major fraction with the FCC conditioning bed (11.56 wt%). A comparison of the reforming performance when olivine and Al_2O_3 conditioning beds are used reveals that both total concentration of the phenolic fraction and component distribution in this faction influence the performance of the reforming catalyst. Accordingly, the presence of guaicols, and especially catechols led to a fast catalyst deactivation in the reforming step.

Despite the stability of G90 catalyst is greatly improved when an Al_2O_3 conditioning catalyst is used, the rapid deactivation of the reforming catalyst will entail working under reaction-regeneration cycles when the operation is performed at large scale.

Fig. 3 shows the evolution of the yields of gaseous product and non-converted bio-oil compounds with time on stream for the experiments conducted without conditioning (Fig. 3a), and with conditioning catalysts (Fig. 3b-e). As observed, H_2 and CO_2 decreased with time on stream

in all cases due to the lower extension of reforming, Eqs. (6) and (9), and WGS reaction, Eq. (7), as the catalyst is being deactivated. The runs conducted without conditioning catalyst and inert sand showed a similar trend in the evolution of gaseous product yields, which is evidence of the similarities in the volatile stream reaching the reforming bed catalyst in both experiments.

When olivine and spent FCC catalysts were used, the evolution with time on stream followed a similar trend as conversion, with a stable H_2 and CO_2 yield for the first 30 min. Regarding the FCC guard bed, a sharp decrease in H_2 and CO_2 yields was observed due to the attenuation of the reforming and WGS reaction (Eqs. (6) and (7), respectively) as the catalyst was being deactivated. In the case of the γ-Al_2O_3 conditioning bed, the yields of H_2 and CO_2 decreased from the beginning of the reaction. Thus, H_2 yield decreased from 95.9 to 28.1 % and CO_2 from 93.9 % to 33.1 % for 112 min on stream.

In all cases, the deactivation rate of the catalyst is faster as the concentration of the non-converted bio-oil compounds in the reaction medium is higher. In fact, an autocatalytic deactivation behaviour has been reported in the reforming of biomass pyrolysis volatiles [58,95]. These results clearly show that the oxygenated compounds, particularly the phenolic fraction (mainly catechols) produced in the pyrolysis of biomass using FCC conditioning bed, cause a much faster deactivation, which reveals that these compounds are the main coke precursors.

The results obtained at zero time on stream for H_2 production (based on the biomass mass unit in the feed) revealed a high performance of the overall pyrolysis-reforming strategy, with values between 9.5 and 10.2 wt%. Similar H_2 production values were reported in a previous study conducted under the same experimental conditions, but using a fluidized bed reactor in the reforming step [26]. Xiao et al. [96] studied the pyrolysis-reforming of pinewood chips on a Ni/coal char catalyst, obtaining a H_2 production of 10 wt% at a reforming temperature of 650 °C. Ma et al. [97] reported a H_2 production value of 7.6 wt% in a three-step process (biomass pyrolysis, gas–solid simultaneous gasification and catalytic reforming) using a Ni/MgO commercial catalyst. Akubo et al. [98] investigated the pyrolysis-catalytic steam reforming of six agricultural biomass waste samples obtaining a H_2 production in the 3.3–5.1 wt% range.

As concerns CO yield, a slightly decreasing trend is observed in all the experimental runs, which is a consequence of a balance involving its production by the reforming reaction (decreasing with time on stream), Eq. (6), formation by cracking reactions, Eq. (8), and deactivation of the catalyst for the WGS reaction, (Eq. (7)). As the reaction proceeded, the yields of CH_4 and light hydrocarbons increased slightly, which is evidence of cracking reactions, although to a minor extent (CH_4 yields lower than 2 %) due to the operating conditions used in the reforming reactor, i.e., rather low temperature and residence time.

3.4. Coke deposition

With the aim of evaluating the influence of different conditioning beds on the pyrolysis volatile composition and their relationship with catalysts performance and deactivation, the cokes deposited on the guard catalysts as well as on the commercial Ni/Al_2O_3 (G90) catalyst have been characterized by temperature programmed oxidation (TPO). The main causes of catalyst deactivation in the reforming processes are metal sintering and coke deposition [99]. However, previous pyrolysis-reforming studies conducted by the research group using the commercial Ni/Al_2O_3 (G90) catalyst evidenced that metal sintering did not occur [100]. Thus, the low reforming temperature used in this study (600 °C) is slightly higher than Ni Tamman temperature (590 °C), and metal sintering is therefore avoided. Accordingly, coke deposition is the main responsible for catalyst deactivation.

3.4.1. Coke deposition on the conditioning catalysts

TPO analyses have been conducted to the guard materials in order to ascertain the influence textural properties and their characteristic features have on the coke deposited. It should be noted that the coke is formed due to the contact of the volatile stream with these materials prior to reaching the reforming catalyst. However, due to the different duration of the runs (which depends on the stability of the G90 catalyst in the reforming step), and in order to compare the amount of coke deposited on each conditioning catalyst, the average coke deposition rate per biomass mass unit has been defined as follows:

$$\bar{r}_{coke} = \frac{W_{coke}/t}{W_{catalyst}\ m_{biomass}} \quad (10)$$

with $W_{catalyst}$ and W_{coke} being the catalyst and coke masses, respectively, $m_{biomass}$ the biomass mass flow rate in the feed and t the reaction time in each run.

The results of coke content and average coke deposition rate per biomass mass unit are set out in Table 5, and the TPO profiles are shown in Fig. 4.

As observed in Table 5, significant differences are observed in the results for the conditioning catalysts used. Thus, the runs conducted with silica sand and olivine led to a negligible amount of coke deposition (0.13 and 0.38 wt%, respectively), which corresponds to average coke deposition rates per biomass mass unit of 0.02 and 0.05 $mg_{coke}\ g_{gc}^{-1}\ g_{biomass}^{-1}$. The limited porous structure of these materials (see Table 2) hindered coke deposition. Their characteristic features, i.e., the inert nature of silica sand, and the basic nature of olivine, as well as the capability of the latter to enhance reforming reactions, may contribute to attenuating coke deposition.

As concerns γ-Al_2O_3 and spent FCC conditioning catalysts, the amounts of coke deposited and the average coke deposition rates per biomass mass unit were considerable higher (0.98 and 2.04 $mg_{coke}\ g_{gc}^{-1}\ g_{biomass}^{-1}$, for FCC and γ-$Al_2O_3$, respectively). It is well-established in the literature that the acid properties of these materials promote the formation of coke deposits due to dehydration, cracking and polymerization reactions, which take place on the acid sites [22,71,94,101,102]. Accordingly, the higher total acidity of the γ-Al_2O_3 compared to the FCC catalyst (See Table 2) led to a higher amount of coke deposited on this conditioning bed. The selective coke deposition on the former conditioning catalyst surface attenuates the subsequent coke formation on the reforming catalyst, and therefore improves its stability. Thus, the coke precursors are deposited on the acid sites of Al_2O_3 conditioning catalyst, leading to a volatile stream less prone to coke formation on the G90

Table 5
Textural properties and values of coke content (C_C) and average coke deposition rate per biomass mass unit (r_C) on the conditioning catalysts (gc) after pyrolysis-reforming runs.

Guard catalyst	S_{BET} ($m^2\ g^{-1}$) *Fresh/spent*	V_{pore} ($cm^3\ g^{-1}$) *Fresh/spent*	d_{pore} (nm) *Fresh/spent*	C_c (gc) (wt%)	r_c (gc) ($mg_{coke}\ g_{gc}^{-1}\ g_{biomass}^{-1}$)
Inert sand	0.6/0.1	-/-	-/-	0.13	0.02
γ-Al_2O_3	100.6/83.9	0.42/0.30	16.9/12.3	17.12	2.04
FCC	81.3/15.1	0.09/0.04	16.8/18.7	5.61	0.98
Olivine	2.4/1.2	0.003/0.003	-/-	0.38	0.05

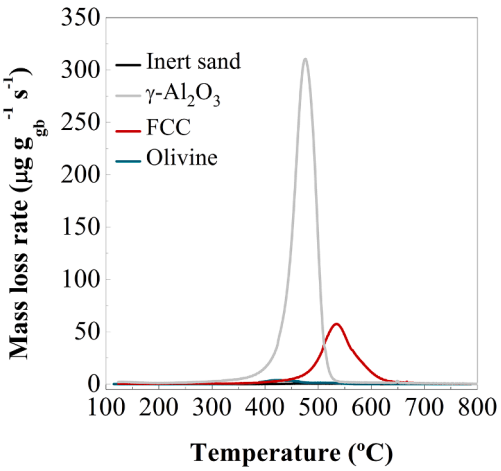

Fig. 4. TPO profiles of the used conditioning catalysts.

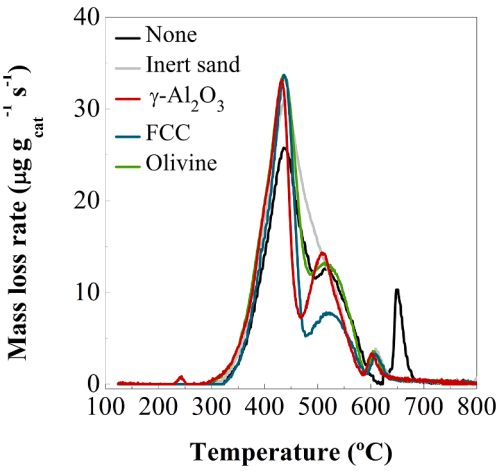

Fig. 5. TPO profiles of the commercial Ni/Al_2O_3 catalyst deactivated using different conditioning beds prior to the reforming process.

reforming catalyst surface. Moreover, the mesoporous structure of these materials favors coke deposition on their surface. Similarly, Li et al. [93] analyzed the main reaction pathways occurring in the catalytic cracking of different bio-oil model compounds (acetic acid, cyclopentanone and guaicol). They reported a higher coke production when guaicol was used, and ascribed it to the coke chemical structure and hydrogen to carbon effective ratios of the feedstock. Besides, these authors describe coke formation as a sequence of polymerization and polycondensation reactions involving bulky aromatic compounds formed in the catalytic cracking of guaicol, which lead to carbon deposits on the catalyst surface.

The textural properties of the fresh and spent conditioning catalysts are also shown in Table 5. As observed, the coke deposited on the conditioning materials also influenced their textural properties. In the case of inert sand and olivine, no significant differences were observed prior and subsequent to use in the pyrolysis-reforming runs due to the limited porous structure of these materials. However, a sharp decrease in the S_{BET} area was observed for the FCC catalyst (from 81.3 to 15.1 $m^2\ g^{-1}$) due the full blockage of the pores, especially the micropores of the HY zeolite structure. Concerning the γ-Al_2O_3 catalyst, the specific surface area and average pore diameter decreased from 100.6 to 83.9 $m^2\ g^{-1}$ and from 16.9 to 12.3 nm, respectively, which is evidence of the partial blockage of the pores in this catalyst.

Fig. 4 shows the TPO profiles of all conditioning catalysts, wherein significant differences are revealed concerning their coke combustion temperature. As regards the γ-Al_2O_3 catalyst, one main peak located at 475 °C is observed, whereas the main peak in the profile of the spent FCC catalyst is located at 535 °C. Thus, cokes of different nature are deposited, with the one deposited on the γ-Al_2O_3 catalyst being more hydrogenated (higher proportion of aliphatic compounds than aromatic ones), whereas that on the FCC catalyst has a more structured aromatic composition [103,104].

3.4.2. Coke deposition on the commercial Ni/Al_2O_3 (G90) catalysts

Table 6 shows the amounts of coke deposited (C_C) and the average coke deposition rates per biomass mass unit fed (r_C) on the deactivated Ni/Al_2O_3 catalysts when different conditioning beds are used prior to the reforming. As in the previous section, this average coke deposition rate has been determined by Eq. (10). As observed, a similar average coke deposition rate was obtained in the experiments conducted without conditioning catalyst and inert sand (0.67 and 0.66 $mg_{coke}\ g_{cat}^{-1}\ g_{biomass}^{-1}$, respectively), which is consistent with their similar evolution of conversion and product yields with time on stream (Figs. 2 and 3, respectively).

The poor performance of the reforming process observed in Fig. 2 when the FCC catalyst was used is supported by the high average coke deposition rate obtained (0.70 $mg_{coke}\ g_{cat}^{-1}\ g_{biomass}^{-1}$). Thus, the composition of the volatile stream reaching the reforming catalyst is responsible for this coke formation rate, and therefore for catalyst deactivation. Accordingly, the high concentration of phenolic compounds (catechols) in the volatile stream when the FCC guard bed is used increases the coke deposition rate.

The lowest average coke deposition rate was obtained when γ-Al_2O_3 was used as guard catalyst, which is consistent with the better performance observed in Fig. 2. The amount of coke deposited on the conditioning catalyst has an influence on the amount of coke deposited on the reforming catalyst. As aforementioned, the higher acidity of the γ-Al_2O_3 favored coke promoters deposition on its surface (see Table 5), and so decreased the coke formation rate on the subsequent Ni/Al_2O_3 (G90) catalyst used in the reforming step. Besides, the composition of the volatile stream to be reformed, with a high fraction of hydrocarbons and the phenolic one containing only alkyl-phenols, attenuates coke deposition. Thus, several authors have reported that oxygenated compounds are more prone to form carbon deposits than aromatic hydrocarbons [47,84].

Regarding the experiments conducted with the olivine conditioning catalyst, a similar average coke deposition rate as in the runs without conditioning bed and with silica sand (0.67 $mg_{coke}\ g_{cat}^{-1}\ g_{biomass}^{-1}$) was observed on the reforming catalyst. Thus, although the conversion of pyrolysis volatiles decreased faster during the initial minutes on stream due to the presence of refractory compounds in the volatile stream, a

Table 6
Values of coke content (C_C) and average coke deposition rate per biomass mass unit (r_C) on the deactivated reforming catalyst (Ni/Al_2O_3 (G90)).

Conditioning catalyst	C_c (Ni/Al_2O_3) (wt%)	r_c (Ni/Al_2O_3) ($mg_{coke}\ g_{cat}^{-1}\ g_{biomass}^{-1}$)	Time on stream (min)	Biomass fed (g)
–	4.33	0.67	86.3	64.7
Inert sand	4.87	0.66	98.3	73.7
γ-Al_2O_3	4.11	0.49	112.0	84.0
FCC	3.97	0.70	76.0	57.0
Olivine	4.93	0.67	98.4	73.8

similar coke formation rate was observed on the Ni/Al_2O_3 reforming catalyst.

It should be noted that use of a fixed bed regime in the reforming step may lead to severe coke formation on both the conditioning and the reforming catalysts, and therefore to operational problems, such as bed plugging [60,105].

Fig. 5 shows the TPO profiles of the deactivated commercial Ni/Al_2O_3 catalyst when different conditioning beds were used prior to the pyrolysis-reforming process. In these profiles, two main peaks can be distinguished in all the catalyst samples, with the first one located at 435 °C (coke I), and the second one at 525 °C (coke II). The different combustion temperatures observed are closely related to the location and/or composition of the coke deposited. Accordingly, the lower combustion temperature (<475 °C) is ascribed to the coke deposited on Ni metallic sites (encapsulating coke with an amorphous nature). This coke fraction hinders the access of reactants to the active sites due to Ni particle encapsulation, and is therefore the main responsible for catalyst deactivation. Besides, this type of coke (coke I) is more hydrogenated, has a higher content of aliphatic compounds than the other one at higher temperature and is stemmed from the decomposition of oxygenates derived from biomass pyrolysis and the re-polymerization of phenolic compounds [58]. The peak located at the higher temperature (coke II) has been related to the coke deposited on the support aside from Ni active sites (and therefore, having less influence on catalyst deactivation), and is composed of highly ordered and condensed aromatic compounds [94,100,106]. Moreover, the SEM images shown for the deactivated G90 catalysts in Fig. S2 in the Supplementary Information, in which no specific morphology of the coke formed is observed, confirm the results obtained by TPO analysis.

In the case the spent FCC catalyst is used as guard bed, the TPO profile of the Ni/Al_2O_3 catalyst reveals a higher proportion of coke I than coke II, which is evidence that it promotes the formation of encapsulating coke, thereby hindering the access of reactants to the metallic sites. Therefore, although coke content has a great influence on catalyst deactivation, coke structure and location also play an essential role on deactivation [94,107]. A minor peak appears at 660 °C in the TPO profile of the G90 catalyst used without any conditioning bed. As aforementioned, G90 catalyst is doped with Ca, and previous studies show that this high combustion temperature peak must be ascribed to the decomposition of $CaCO_3$, which is formed by carbonation of the CaO contained in the commercial G90 catalyst [48]. Furthermore, all the conditioning catalysts used in the pyrolysis-reforming process led to a small peak at 610 °C, which arose from the thermal cracking of hydrocarbons or oxygenates in the reaction medium [94].

4. Conclusions

Improvements have been carried out in an integrated reaction system for H_2 production from biomass consisting of a conical spouted bed reactor for the fast pyrolysis and an in-line fixed bed reactor for the steam reforming of the oxygenate volatile stream. Thus, it has been proven that the provision of low cost conditioning catalysts (γ-Al_2O_3, spent FCC catalyst and olivine) prior to the reforming reactor allows tempering the volatile stream, and therefore modifying oxygenate composition, which enables the attenuation of the fast deactivation of the reforming catalyst (G90).

Coke deposition is the main cause of catalyst deactivation, which leads to the blockage of the Ni active sites. Phenolic compounds in the oxygenate stream, and especially the presence of guaiacols and catechols, have a considerable influence on coke formation due to the repolymeration of these compounds on the Ni sites. This coke has been identified by TPO analysis due to its low combustion temperature.

Based on the results and features of the conditioning catalysts, it has been proven that the high total acidity of γ-Al_2O_3 (with a high density of centers and moderate acid strength) is suitable for the selective cracking of the volatile fraction responsible for coke formation. Thus, although the initial H_2 production decreases when γ-Al_2O_3 is used as conditioning catalyst, the stability of the reforming G90 catalyst is enhanced, and therefore a longer duration of the reaction stage is feasible.

Although the deactivation of the catalyst is notably attenuated with this strategy, the deactivation by coke deposition of the conditioning catalyst is also observed. Consequently, the scalability of this two-step pyrolysis-reforming process provided with a conditioning step will require regeneration strategies for both the G90 reforming catalyst and the γ-Al_2O_3 conditioning catalyst.

CRediT authorship contribution statement

Enara Fernandez: Investigation, Visualization, Writing – review & editing. **Laura Santamaria:** Writing – original draft, Visualization, Writing – review & editing. **Maite Artetxe:** Writing – original draft, Conceptualization, Writing – review & editing, Visualization, Supervision, Project administration, Funding acquisition. **Maider Amutio:** Conceptualization, Writing – review & editing, Visualization, Supervision, Project administration, Funding acquisition. **Aitor Arregi:** Validation, Visualization, Writing – review & editing. **Gartzen Lopez:** Conceptualization, Validation, Writing – review & editing, Visualization, Supervision, Project administration. **Javier Bilbao:** Writing – review & editing, Visualization, Supervision, Project administration, Funding acquisition. **Martin Olazar:** Writing – review & editing, Visualization, Supervision, Project administration, Funding acquisition.

Declaration of Competing Interest

The authors declare that they have no known competing financial interests or personal relationships that could have appeared to influence the work reported in this paper.

Acknowledgement

This work was carried out with the financial support of the grants RTI2018-101678-B-I00, RTI2018-098283-J-I00 and PID2019-107357RB-I00 funded by MCIN/AEI/ 10.13039/501100011033 and by “ERDF A way of making Europe” and the grants IT1218-19 and KK-2020/00107 funded by the Basque Government. Moreover, this project has received funding from the European Union’s Horizon 2020 research and innovation programme under the Marie Sklodowska-Curie grant agreement No 823745.

Appendix A. Supplementary data

Supplementary data to this article can be found online at https://doi.org/10.1016/j.fuel.2021.122910.

References

[1] Hosseini SE, Wahid MA. Hydrogen production from renewable and sustainable energy resources: Promising green energy carrier for clean development. Renewable Sustainable Energy Rev 2016;57:850–66. https://doi.org/10.1016/j.rser.2015.12.112.

[2] Schmitt N, Apfelbacher A, Jäger N, Daschner R, Stenzel F, Hornung A. Thermochemical conversion of biomass and upgrading to biofuel: the thermo-catalytic reforming process – a review. Biofuels, Bioprod Biorefin 2019;13(3):822–37. https://doi.org/10.1002/bbb.1980.

[3] Ma J, Shi S, Jia X, Xia F, Ma H, Gao J, et al. Advances in catalytic conversion of lignocellulose to chemicals and liquid fuels. J Energy Chem 2019;36:74–86. https://doi.org/10.1016/j.jechem.2019.04.026.

[4] Ren J, Cao J-P, Zhao X-Y, Liu Y-L. Fundamentals and applications of char in biomass tar reforming. Fuel Process Technol 2021;216:106782. https://doi.org/10.1016/j.fuproc.2021.106782.

[5] Balat H, Kırtay E. Hydrogen from biomass – present scenario and future prospects. Int J Hydrogen Energy 2010;35(14):7416–26. https://doi.org/10.1016/j.ijhydene.2010.04.137.

[6] Levin DB, Chahine R. Challenges for renewable hydrogen production from biomass. Int J Hydrogen Energy 2010;35(10):4962–9. https://doi.org/10.1016/j.ijhydene.2009.08.067.

[7] Karl J, Pröll T. Steam gasification of biomass in dual fluidized bed gasifiers: a review. Renewable Sustainable Energy Rev 2018;98:64–78. https://doi.org/10.1016/j.rser.2018.09.010.

[8] Arregi A, Amutio M, Lopez G, Bilbao J, Olazar M. Evaluation of thermochemical routes for hydrogen production from biomass: a review. Energy Convers Manage 2018;165:696–719. https://doi.org/10.1016/j.enconman.2018.03.089.

[9] Pandey B, Prajapati YK, Sheth PN. Recent progress in thermochemical techniques to produce hydrogen gas from biomass: a state of the art review. Int J Hydrogen Energy 2019;44(47):25384–415. https://doi.org/10.1016/j.ijhydene.2019.08.031.

[10] Melero JA, Iglesias J, Garcia A. Biomass as renewable feedstock in standard refinery units. Feasibility, opportunities and challenges. Energy. Environ Sci 2012;5:7393–420. https://doi.org/10.1039/c2ee21231e.

[11] Ni M, Leung DYC, Leung MKH, Sumathy K. An overview of hydrogen production from biomass. Fuel Process Technol 2006;87(5):461–72. https://doi.org/10.1016/j.fuproc.2005.11.003.

[12] Das D, Veziroglu T. Advances in biological hydrogen production processes. Int J Hydrogen Energy 2008;33(21):6046–57. https://doi.org/10.1016/j.ijhydene.2008.07.098.

[13] Dou B, Zhang H, Song Y, Zhao L, Jiang B, He M, et al. Hydrogen production from the thermochemical conversion of biomass: issues and challenges. Sustainable Energy Fuels 2019;3(2):314–42. https://doi.org/10.1039/C8SE00535D.

[14] Pang S. Advances in thermochemical conversion of woody biomass to energy, fuels and chemicals. Biotechnol Adv 2019;37(4):589–97. https://doi.org/10.1016/j.biotechadv.2018.11.004.

[15] Molino A, Chianese S, Musmarra D. Biomass gasification technology: The state of the art overview. J Energy Chem 2016;25(1):10–25. https://doi.org/10.1016/j.jechem.2015.11.005.

[16] Sikarwar VS, Zhao M, Clough P, Yao J, Zhong X, Memon MZ, et al. An overview of advances in biomass gasification. Energy Environ Sci 2016;9(10):2939–77.

[17] Mahinpey N, Gomez A. Review of gasification fundamentals and new findings: reactors, feedstock, and kinetic studies. Chem Eng Sci 2016;148:14–31. https://doi.org/10.1016/j.ces.2016.03.037.

[18] Cortazar M, Alvarez J, Lopez G, Amutio M, Santamaria L, Bilbao J, et al. Role of temperature on gasification performance and tar composition in a fountain enhanced conical spouted bed reactor. Energy Convers Manage 2018;171:1589–97. https://doi.org/10.1016/j.enconman.2018.06.071.

[19] Ren J, Cao J-P, Zhao X-Y, Yang F-L, Wei X-Y. Recent advances in syngas production from biomass catalytic gasification: a critical review on reactors, catalysts, catalytic mechanisms and mathematical models. Renewable Sustainable Energy Rev 2019;116:109426. https://doi.org/10.1016/j.rser.2019.109426.

[20] Chen Xu, Che Q, Li S, Liu Z, Yang H, Chen Y, et al. Recent developments in lignocellulosic biomass catalytic fast pyrolysis: Strategies for the optimization of bio-oil quality and yield. Fuel Process Technol 2019;196:106180. https://doi.org/10.1016/j.fuproc.2019.106180.

[21] Fahmy TYA, Fahmy Y, Mobarak F, El-Sakhawy M, Abou-Zeid RE. Biomass pyrolysis: past, present, and future. Environ Dev Sustainability 2020;22(1):17–32. https://doi.org/10.1007/s10668-018-0200-5.

[22] Chen J, Sun J, Wang Y. Catalysts for steam reforming of bio-oil: a review. Ind Eng Chem Res 2017;56(16):4627–37. https://doi.org/10.1021/acs.iecr.7b00600.

[23] Zhao Z, Situmorang YA, An P, Chaihad N, Wang J, Hao X, et al. Hydrogen production from catalytic steam reforming of bio-oils: a critical review. Chem Eng Technol 2020;43(4):625–40. https://doi.org/10.1002/ceat.201900487.

[24] Gao N, Quan C, Ma Z, Wu C. Thermal characteristics of biomass pyrolysis oil and potential hydrogen production by catalytic steam reforming. Energy Fuels 2018;32(4):5234–43. https://doi.org/10.1021/acs.energyfuels.8b00365.

[25] Gao N, Han Y, Quan C, Wu C. Promoting hydrogen-rich syngas production from catalytic reforming of biomass pyrolysis oil on nanosized nickel-ceramic catalysts. Appl Therm Eng 2017;125:297–305. https://doi.org/10.1016/j.applthermaleng.2017.07.028.

[26] Arregi A, Lopez G, Amutio M, Barbarias I, Bilbao J, Olazar M. Hydrogen production from biomass by continuous fast pyrolysis and in-line steam reforming. RSC Adv 2016;6(31):25975–85.

[27] Liu Y, Yu H, Liu J, Chen D. Catalytic characteristics of innovative Ni/slag catalysts for syngas production and tar removal from biomass pyrolysis. Int J Hydrogen Energy 2019;44(23):11848–60. https://doi.org/10.1016/j.ijhydene.2019.03.024.

[28] Yu H, Liu Y, Liu J, Chen D. High catalytic performance of an innovative Ni/magnesium slag catalyst for the syngas production and tar removal from biomass pyrolysis. Fuel 2019;254:115622. https://doi.org/10.1016/j.fuel.2019.115622.

[29] Kumagai S, Alvarez J, Blanco PH, Wu C, Yoshioka T, Olazar M, et al. Novel Ni–Mg–Al–Ca catalyst for enhanced hydrogen production for the pyrolysis–gasification of a biomass/plastic mixture. J Anal Appl Pyrolysis 2015;113:15–21. https://doi.org/10.1016/j.jaap.2014.09.012.

[30] Tang W, Cao J-P, Yang F-L, Feng X-B, Ren J, Wang J-X, et al. Highly active and stable HF acid modified HZSM-5 supported Ni catalysts for steam reforming of toluene and biomass pyrolysis tar. Energy Convers Manage 2020;212:112799. https://doi.org/10.1016/j.enconman.2020.112799.

[31] Arregi A, Lopez G, Amutio M, Barbarias I, Santamaria L, Bilbao J, et al. Regenerability of a Ni catalyst in the catalytic steam reforming of biomass pyrolysis volatiles. J Ind Eng Chem 2018;68:69–78. https://doi.org/10.1016/j.jiec.2018.07.030.

[32] Soomro A, Chen S, Ma S, Xiang W. Catalytic activities of nickel, dolomite, and olivine for tar removal and H2-enriched gas production in biomass gasification process. Energy Environ 2018;29(6):839–67. https://doi.org/10.1177/0958305X18767848.

[33] Shen Y, Yoshikawa K. Recent progresses in catalytic tar elimination during biomass gasification or pyrolysis — A review. Renewable Sustainable Energy Rev 2013;21:371–92. https://doi.org/10.1016/j.rser.2012.12.062.

[34] Islam MW. A review of dolomite catalyst for biomass gasification tar removal. Fuel 2020;267:117095. https://doi.org/10.1016/j.fuel.2020.117095.

[35] Cortazar M, Santamaria L, Lopez G, Alvarez J, Amutio M, Bilbao J, et al. Fe/olivine as primary catalyst in the biomass steam gasification in a fountain confined spouted bed reactor. J Ind Eng Chem 2021;99:364–79. https://doi.org/10.1016/j.jiec.2021.04.046.

[36] Abu El-Rub Z, Bramer EA, Brem G. Review of catalysts for tar elimination in biomass gasification processes. Ind Eng Chem Res 2004;43(22):6911–9. https://doi.org/10.1021/ie0498403.

[37] Hanchate N, Ramani S, Mathpati CS, Dalvi VH. Biomass gasification using dual fluidized bed gasification systems: a review. J Clean Prod 2021;280:123148. https://doi.org/10.1016/j.jclepro.2020.123148.

[38] Kuramoto K, Matsuoka K, Murakami T, Takagi H, Nanba T, Suzuki Y, et al. Cracking and coking behaviors of nascent volatiles derived from flash pyrolysis of woody biomass over mesoporous fluidized-bed material. Ind Eng Chem Res 2009;48(6):2851–60. https://doi.org/10.1021/ie800760s.

[39] Cortazar M, Lopez G, Alvarez J, Amutio M, Bilbao J, Olazar M. Behaviour of primary catalysts in the biomass steam gasification in a fountain confined spouted bed. Fuel 2019;253:1446–56. https://doi.org/10.1016/j.fuel.2019.05.094.

[40] Abu El-Rub Z, Bramer EA, Brem G. Experimental comparison of biomass chars with other catalysts for tar reduction. Fuel 2008;87(10-11):2243–52. https://doi.org/10.1016/j.fuel.2008.01.004.

[41] Li D, Tamura M, Nakagawa Y, Tomishige K. Metal catalysts for steam reforming of tar derived from the gasification of lignocellulosic biomass. Bioresour Technol 2015;178:53–64. https://doi.org/10.1016/j.biortech.2014.10.010.

[42] Nabgan W, Tuan Abdullah TA, Mat R, Nabgan B, Gambo Y, Ibrahim M, et al. Renewable hydrogen production from bio-oil derivative via catalytic steam reforming: An overview. Renewable Sustainable Energy Rev 2017;79:347–57. https://doi.org/10.1016/j.rser.2017.05.069.

[43] Santamaria L, Lopez G, Arregi A, Artetxe M, Amutio M, Bilbao J, et al. Catalytic steam reforming of biomass fast pyrolysis volatiles over Ni–Co bimetallic catalysts. J Ind Eng Chem 2020;91:167–81. https://doi.org/10.1016/j.jiec.2020.07.050.

[44] Li X, Zhang Z, Zhang L, Fan H, Li X, Liu Q, et al. Investigation of coking behaviors of model compounds in bio-oil during steam reforming. Fuel 2020;265:116961. https://doi.org/10.1016/j.fuel.2019.116961.

[45] Nabgan W, Tuan Abdullah TA, Mat R, Nabgan B, Gambo Y, Moghadamian K. Acetic acid-phenol steam reforming for hydrogen production: Effect of different composition of La_2O_3-Al_2O_3 support for bimetallic Ni-Co catalyst. J Environ Chem Eng 2016;4(3):2765–73.

[46] Polychronopoulou K, Costa CN, Efstathiou AM. The steam reforming of phenol reaction over supported-Rh catalysts. Appl Catal, A 2004;272(1-2):37–52. https://doi.org/10.1016/j.apcata.2004.05.002.

[47] Artetxe M, Alvarez J, Nahil MA, Olazar M, Williams PT. Steam reforming of different biomass tar model compounds over Ni/Al_2O_3 catalysts. Energy Convers Manage 2017;136:119–26. https://doi.org/10.1016/j.enconman.2016.12.092.

[48] Fernandez E, Amutio M, Artetxe M, Arregi A, Santamaria L, Lopez G, et al. Assessment of product yields and catalyst deactivation in fixed and fluidized bed reactors in the steam reforming of biomass pyrolysis volatiles. Process Saf Environ Prot 2021;145:52–62. https://doi.org/10.1016/j.psep.2020.07.039.

[49] Amutio M, Lopez G, Artetxe M, Elordi G, Olazar M, Bilbao J. Influence of temperature on biomass pyrolysis in a conical spouted bed reactor. Resour Conserv Recycl 2012;59:23–31. https://doi.org/10.1016/j.resconrec.2011.04.002.

[50] Cao J, Ren J, Zhao X, Wei X, Takarada T. Effect of atmosphere on carbon deposition of Ni/Al_2O_3 and Ni-loaded on lignite char during reforming of toluene as a biomass tar model compound. Fuel 2018;217:515–21. https://doi.org/10.1016/j.fuel.2017.12.121.

[51] Oh G, Park SY, Seo MW, Kim YK, Ra HW, Lee J-G, et al. Ni/Ru–Mn/Al_2O_3 catalysts for steam reforming of toluene as model biomass tar. Renewable Energy 2016;86:841–7. https://doi.org/10.1016/j.renene.2015.09.013.

[52] Kannari N, Oyama Y, Takarada T. Catalytic decomposition of tar derived from biomass pyrolysis using Ni-loaded chicken dropping catalysts. Int J Hydrogen Energy 2017;42(15):9611–8. https://doi.org/10.1016/j.ijhydene.2017.02.168.

[53] Wang B-S, Cao J-P, Zhao X-Y, Bian Y, Song C, Zhao Y-P, et al. Preparation of nickel-loaded on lignite char for catalytic gasification of biomass. Fuel Process Technol 2015;136:17–24. https://doi.org/10.1016/j.fuproc.2014.07.024.

[54] Cao JP, Shi P, Zhao XY, Wei XY, Takarada T. Catalytic reforming of volatiles and nitrogen compounds from sewage sludge pyrolysis to clean hydrogen and synthetic gas over a nickel catalyst. Fuel Process Technol 2014;123:34–40. https://doi.org/10.1016/j.fuproc.2014.01.042.

[55] Kawamoto K, Wu W, Kuramochi H. Development of gasification and reforming technology using catalyst at lower temperature for effective energy recovery: Hydrogen recovery using waste wood. J Environ Eng 2009;4(2):409–21. https://doi.org/10.1299/jee.4.409.

[56] Wu W, Kawamoto K, Kuramochi H. Hydrogen-rich synthesis gas production from waste wood via gasification and reforming technology for fuel cell application. J Mater Cycles Waste Manage 2006;8(1):70–7. https://doi.org/10.1007/s10163-005-0138-1.

[57] Tsuji T, Okajima S, Sasaki A, Masuda T. Steam reforming of oils produced from waste plastics. J Chem Eng Jpn 2005;38(10):859–64. https://doi.org/10.1252/jcej.38.859.

[58] Arregi A, Lopez G, Amutio M, Artetxe M, Barbarias I, Bilbao J, et al. Role of operating conditions in the catalyst deactivation in the in-line steam reforming of volatiles from biomass fast pyrolysis. Fuel 2018;216:233–44. https://doi.org/10.1016/j.fuel.2017.12.002.

[59] Santamaria L, Arregi A, Lopez G, Artetxe M, Amutio M, Bilbao J, et al. Effect of La_2O_3 promotion on a Ni/Al_2O_3 catalyst for H_2 production in the in-line biomass pyrolysis-reforming. Fuel 2020;262:116593. https://doi.org/10.1016/j.fuel.2019.116593.

[60] Erkiaga A, Lopez G, Barbarias I, Artetxe M, Amutio M, Bilbao J, et al. HDPE pyrolysis-steam reforming in a tandem spouted bed-fixed bed reactor for H_2 production. J Anal Appl Pyrolysis 2015;116:34–41. https://doi.org/10.1016/j.jaap.2015.10.010.

[61] Lopez G, Erkiaga A, Artetxe M, Amutio M, Bilbao J, Olazar M. Hydrogen production by high density polyethylene steam gasification and in-line volatile reforming. Ind Eng Chem Res 2015;54(39):9536–44. https://doi.org/10.1021/acs.iecr.5b02413.

[62] Alvarez J, Lopez G, Amutio M, Bilbao J, Olazar M. Bio-oil production from rice husk fast pyrolysis in a conical spouted bed reactor. Fuel 2014;128:162–9. https://doi.org/10.1016/j.fuel.2014.02.074.

[63] Amutio M, Lopez G, Alvarez J, Olazar M, Bilbao J. Fast pyrolysis of eucalyptus waste in a conical spouted bed reactor. Bioresour Technol 2015;194:225–32. https://doi.org/10.1016/j.biortech.2015.07.030.

[64] Artetxe M, Lopez G, Amutio M, Barbarias I, Arregi A, Aguado R, et al. Styrene recovery from polystyrene by flash pyrolysis in a conical spouted bed reactor. Waste Manage 2015;45:126–33. https://doi.org/10.1016/j.wasman.2015.05.034.

[65] Artetxe M, Lopez G, Elordi G, Amutio M, Bilbao J, Olazar M. Production of light olefins from polyethylene in a two-step process: Pyrolysis in a conical spouted bed and downstream high-temperature thermal cracking. Ind Eng Chem Res 2012;51(43):13915–23. https://doi.org/10.1021/ie300178e.

[66] Alvarez J, Lopez G, Amutio M, Mkhize NM, Danon B, van der Gryp P, et al. Evaluation of the properties of tyre pyrolysis oils obtained in a conical spouted bed reactor. Energy 2017;128:463–74. https://doi.org/10.1016/j.energy.2017.03.163.

[67] Alvarez J, Amutio M, Lopez G, Santamaria L, Bilbao J, Olazar M. Improving bio-oil properties through the fast co-pyrolysis of lignocellulosic biomass and waste tyres. Waste Manage 2019;85:385–95. https://doi.org/10.1016/j.wasman.2019.01.003.

[68] Lopez G, Alvarez J, Amutio M, Mkhize NM, Danon B, van der Gryp P, et al. Waste truck-tyre processing by flash pyrolysis in a conical spouted bed reactor. Energy Convers Manage 2017;142:523–32. https://doi.org/10.1016/j.enconman.2017.03.051.

[69] Olazar M, San Jose MJ, Penas FJ, Aguayo AT, Bilbao J. Stability and hydrodynamics of conical spouted beds with binary mixtures. Ind Eng Chem Res 1993;32(11):2826–34. https://doi.org/10.1021/ie00023a053.

[70] Santamaria L, Lopez G, Arregi A, Amutio M, Artetxe M, Bilbao J, et al. Stability of different Ni supported catalysts in the in-line steam reforming of biomass fast pyrolysis volatiles. Appl Catal, B 2019;242:109–20. https://doi.org/10.1016/j.apcatb.2018.09.081.

[71] Valle B, Remiro A, García-Gómez N, Gayubo AG, Bilbao J. Recent research progress on bio-oil conversion into bio-fuels and raw chemicals: a review. J Chem Technol Biotechnol 2019;94(3):670–89. https://doi.org/10.1002/jctb.5758.

[72] Elordi G, Olazar M, Castaño P, Artetxe M, Bilbao J. Polyethylene cracking on a spent FCC catalyst in a conical spouted bed. Ind Eng Chem Res 2012;51(43):14008–17. https://doi.org/10.1021/ie3018274.

[73] Rapagnà S, Jand N, Kiennemann A, Foscolo PU. Steam-gasification of biomass in a fluidised-bed of olivine particles. Biomass Bioenergy 2000;19:187–97. https://doi.org/10.1016/S0961-9534(00)00031-3.

[74] Hu G, Xu S, Li S, Xiao C, Liu S. Steam gasification of apricot stones with olivine and dolomite as downstream catalysts. Fuel Process Technol 2006;87(5):375–82. https://doi.org/10.1016/j.fuproc.2005.07.008.

[75] Morin M, Nitsch X, Pécate S, Hémati M. Tar conversion over olivine and sand in a fluidized bed reactor using toluene as model compound. Fuel 2017;209:25–34. https://doi.org/10.1016/j.fuel.2017.07.084.

[76] Fernandez E, Santamaria L, Artetxe M, Amutio M, Arregi A, Lopez G, et al. In line upgrading of biomass fast pyrolysis products using low-cost catalysts. Fuel 2021;296:120682. https://doi.org/10.1016/j.fuel.2021.120682.

[77] Bridgwater AV, Peacocke GVC. Fast pyrolysis processes for biomass. Renewable Sustainable Energy Rev 2000;4:1–73. https://doi.org/10.1016/S1364-0321(99)00007-6.

[78] Mohan D, Pittman Jr CU, Steele PH. Pyrolysis of wood/biomass for bio-oil: a critical review. Energy Fuels 2006;20:848–89. https://doi.org/10.1021/ef0502397.

[79] Hassan NS, Jalil AA, Hitam CNC, Vo DVN, Nabgan W. Biofuels and renewable chemicals production by catalytic pyrolysis of cellulose: a review. Environ Chem Lett 2020;18(5):1625–48. https://doi.org/10.1007/s10311-020-01040-7.

[80] Fernandez E, Santamaria L, Amutio M, Artetxe M, Arregi A, Lopez G, et al. Role of temperature in the biomass steam pyrolysis in a conical spouted bed reactor. Energy 2022;238:122053. https://doi.org/10.1016/j.energy.2021.122053.

[81] Ro D, Kim Y-M, Lee I-G, Jae J, Jung S-C, Kim SC, et al. Bench scale catalytic fast pyrolysis of empty fruit bunches over low cost catalysts and HZSM-5 using a fixed bed reactor. J Clean Prod 2018;176:298–303. https://doi.org/10.1016/j.jclepro.2017.12.075.

[82] Liu C, Wang H, Karim AM, Sun J, Wang Y. Catalytic fast pyrolysis of lignocellulosic biomass. Chem Soc Rev 2014;43(22):7594–623.

[83] Remón J, Broust F, Volle G, García L, Arauzo J. Hydrogen production from pine and poplar bio-oils by catalytic steam reforming. Influence of the bio-oil composition on the process. Int J Hydrogen Energy 2015;40(16):5593–608. https://doi.org/10.1016/j.ijhydene.2015.02.117.

[84] Czernik S, Evans R, French R. Hydrogen from biomass-production by steam reforming of biomass pyrolysis oil. Catal Today 2007;129(3-4):265–8. https://doi.org/10.1016/j.cattod.2006.08.071.

[85] Arregi A, Amutio M, Lopez G, Artetxe M, Alvarez J, Bilbao J, et al. Hydrogen-rich gas production by continuous pyrolysis and in-line catalytic reforming of pine wood waste and HDPE mixtures. Energy Convers Manage 2017;136:192–201. https://doi.org/10.1016/j.enconman.2017.01.008.

[86] Gayubo AG, Aguayo AT, Atutxa A, Valle B, Bilbao J. Undesired components in the transformation of biomass pyrolysis oil into hydrocarbons on an HZSM-5 zeolite catalyst. J Chem Technol Biotechnol 2005;80(11):1244–51. https://doi.org/10.1002/jctb.1316.

[87] Valle B, García-Gómez N, Arandia A, Remiro A, Bilbao J, Gayubo AG. Effect of phenols extraction on the behavior of Ni-spinel derived catalyst for raw bio-oil steam reforming. Int J Hydrogen Energy 2019;44(25):12593–603. https://doi.org/10.1016/j.ijhydene.2018.12.057.

[88] Ochoa A, Aramburu B, Valle B, Resasco DE, Bilbao J, Gayubo AG, et al. Role of oxygenates and effect of operating conditions in the deactivation of a Ni supported catalyst during the steam reforming of bio-oil. Green Chem 2017;19(18):4315–33.

[89] Trane-Restrup R, Jensen AD. Steam reforming of cyclic model compounds of bio-oil over Ni-based catalysts: product distribution and carbon formation. Appl Catal, B 2015;165:117–27. https://doi.org/10.1016/j.apcatb.2014.09.026.

[90] Wang S, Li X, Zhang F, Cai Q, Wang Y, Luo Z. Bio-oil catalytic reforming without steam addition: application to hydrogen production and studies on its mechanism. Int J Hydrogen Energy 2013;38(36):16038–47. https://doi.org/10.1016/j.ijhydene.2013.10.032.

[91] Coll R, Salvadó J, Farriol X, Montané D. Steam reforming model compounds of biomass gasification tars: conversion at different operating conditions and tendency towards coke formation. Fuel Process Technol 2001;74(1):19–31. https://doi.org/10.1016/S0378-3820(01)00214-4.

[92] Josuinkas FM, Quitete CPB, Ribeiro NFP, Souza MMVM. Steam reforming of model gasification tar compounds over nickel catalysts prepared from hydrotalcite precursors. Fuel Process Technol 2014;121:76–82. https://doi.org/10.1016/j.fuproc.2014.01.007.

[93] Li S, Zhang S, Feng Z, Yan Y. Coke formation in the catalytic cracking of bio-oil model compounds. Environ Prog Sustainable Energy 2015;34(1):240–7. https://doi.org/10.1002/ep.11936.

[94] Ochoa A, Bilbao J, Gayubo AG, Castaño P. Coke formation and deactivation during catalytic reforming of biomass and waste pyrolysis products: a review. Renewable Sustainable Energy Rev 2020;119:109600. https://doi.org/10.1016/j.rser.2019.109600.

[95] Santamaria L, Lopez G, Arregi A, Amutio M, Artetxe M, Bilbao J, et al. Effect of calcination conditions on the performance of $Ni/MgO\text{-}Al_2O_3$ catalysts in the steam reforming of biomass fast pyrolysis volatiles. Catal Sci Technol 2019;9(15):3947–63.

[96] Xiao X, Cao J, Meng X, Le DD, Li L, Ogawa Y, et al. Synthesis gas production from catalytic gasification of waste biomass using nickel-loaded brown coal char. Fuel 2013;103:135–40. https://doi.org/10.1016/j.fuel.2011.06.077.

[97] Ma Z, Zhang S-P, Xie D-Y, Yan Y-J. A novel integrated process for hydrogen production from biomass. Int J Hydrogen Energy 2014;39(3):1274–9. https://doi.org/10.1016/j.ijhydene.2013.10.146.

[98] Akubo K, Nahil MA, Williams PT. Pyrolysis-catalytic steam reforming of agricultural biomass wastes and biomass components for production of hydrogen/syngas. J Energy Inst 2019;92(6):1987–96. https://doi.org/10.1016/j.joei.2018.10.013.

[99] Argyle MD, Bartholomew CH. Heterogeneous catalyst deactivation and regeneration: a review. Catalysts 2015;5:145–269. https://doi.org/10.3390/catal5010145.

[100] Ochoa A, Arregi A, Amutio M, Gayubo AG, Olazar M, Bilbao J, et al. Coking and sintering progress of a Ni supported catalyst in the steam reforming of biomass pyrolysis volatiles. Appl Catal, B 2018;233:289–300. https://doi.org/10.1016/j.apcatb.2018.04.002.

[101] Trane R, Dahl S, Skjøth-Rasmussen MS, Jensen AD. Catalytic steam reforming of bio-oil. Int J Hydrogen Energy 2012;37(8):6447–72. https://doi.org/10.1016/j.ijhydene.2012.01.023.

[102] Gac W, Greluk M, Słowik G, Millot Y, Valentin L, Dzwigaj S. Effects of dealumination on the performance of Ni-containing BEA catalysts in bioethanol steam reforming. Appl Catal, B 2018;237:94–109. https://doi.org/10.1016/j.apcatb.2018.05.040.

[103] Ochoa A, Valle B, Resasco DE, Bilbao J, Gayubo AG, Castaño P. Temperature programmed oxidation coupled with in situ techniques reveal the nature and location of coke deposited on a $Ni/La_2O_3\text{-}\alpha Al_2O_3$ catalyst in the steam reforming of bio-oil. ChemCatChem 2018;10:2311–21. https://doi.org/10.1002/cctc.201701942.

[104] Ibáñez M, Valle B, Bilbao J, Gayubo AG, Castaño P. Effect of operating conditions on the coke nature and HZSM-5 catalysts deactivation in the transformation of crude bio-oil into hydrocarbons. Catal Today 2012;195(1):106–13. https://doi.org/10.1016/j.cattod.2012.04.030.

[105] Medrano JA, Oliva M, Ruiz J, García L, Arauzo J. Hydrogen from aqueous fraction of biomass pyrolysis liquids by catalytic steam reforming in fluidized bed. Energy 2011;36(4):2215–24. https://doi.org/10.1016/j.energy.2010.03.059.
[106] Santamaria L, Artetxe M, Lopez G, Cortazar M, Amutio M, Bilbao J, et al. Effect of CeO_2 and MgO promoters on the performance of a Ni/Al_2O_3 catalyst in the steam reforming of biomass pyrolysis volatiles. Fuel Process Technol 2020;198:106223. https://doi.org/10.1016/j.fuproc.2019.106223.
[107] Trane-Restrup R, Resasco DE, Jensen AD. Steam reforming of light oxygenates. Catal Sci Technol 2013;3:3292–302. https://doi.org/10.1039/c3cy00635b.